Supporting Information

A Donor-Acceptor Type Macrocycle: Toward Photolyzable Self-Assembly

Tian Tian,[a] Tingjuan Qian,[a] Tingting Jiang,[a] Yakui Deng,[a] Xiaopei Li,[a] Wei Yuan,[a] Yulan Chen,*[a,b] Yi-Xuan Wang,*[a,b] and Wenping Hu[a,b]

[a]Tianjin Key Laboratory of Molecular Optoelectronic Sciences, Department of Chemistry, School of Science, Tianjin University, Tianjin 300072, P. R. China.

[b]Collaborative Innovation Center of Chemical Science and Engineering (Tianjin), Tianjin 300072, P. R. China.

Contents

1. Experimental information

Unless otherwise noted, commercially available reagents were used without further purification. All the aqueous solution was tested at pH 7.0. The solution for irradiation was placed in cuvette, and further irradiated using a 300W Xenon lamp (CEL-HXF300) with a 365 nm bandpass filter. Nuclear magnetic resonance (NMR) spectra were recorded on a Bruker ADVANCE 400 at 25 °C. In 1D and 2D NMR tests for complexes, a mixture of D_2O and CD_3OD (9:1, v/v) was used as the solvent for better solvation. In NMR titration and Job plot experiments, CH_3CN was used as internal reference. The Electrospray Ionization Mass Spectra (EI-MS) were recorded on a SHIMADZU GCMS-QP2010 SE. MALDI-TOF mass spectra were recorded on a Bruker New Autoflex Speed LIN Spectrometer. High-resolution electrospray ionization mass spectra (HR-ESI-MS) were measured using a Bruker mior OTOF-QII spectrometer. The UV−vis spectra were obtained on a PerkinElmer Lambda 750 spectrophotometer with a temperature controller to keep the temperature at 25 °C. Fluorescence spectra were recorded on a Hitachi model F-7000 spectrofluorometer. The working electrode in cyclic voltammetry experiments (CHI660E B14511 electrochemical workstation) was glassy carbon electrode. The counter electrode was Pt coil. And the reference electrode was Ag/AgCl electrode. The scanning electron microscope (SEM) was recorded with FESEM, JSM-6700F, JEOL. The dynamic laser scattering (DLS) experiment was measured with by NanoBrook 173 plus at scattering angle of 90° at 25 °C. The single crystal structure was determined on Rigaku XtaLAB FRX. A complex solution of AnMV−PTS at 1:1 molar ratio in water was prepared and volatilized to air at 0 °C, from which dark blue crystals were obtained. All DFT calculations were carried out with the Gaussian 09 package.[S1] The B3LYP[S2] functional and a basis set of 6-31G* was used for geometry optimization and frequency calculation. Frequency outcome was analyzed to confirm stationary points as minima (no imaginary frequencies). Computing time was generously provided by the High Performance Computing Center of Tianjin University.

2. Synthesis of AnMV and MVOH

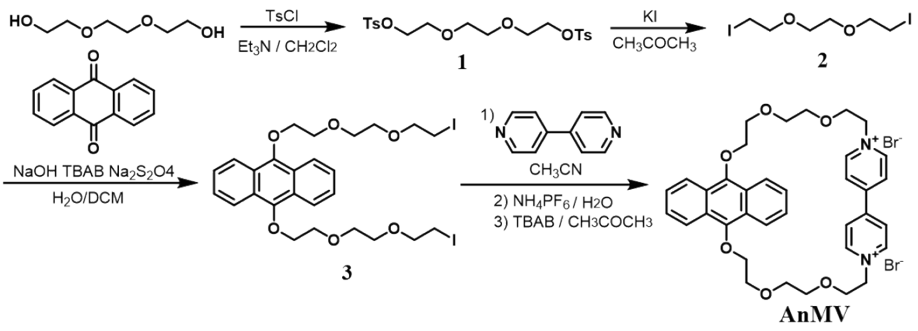

Scheme S1. Synthesis of **AnMV**.

Synthesis of Compounds 1–3. The compounds **1**,[S3] **2**,[S4] and **3**[S5] were synthesized according to literature procedures. Compound **1**: ^{1}H NMR (400 MHz, $CDCl_3$): δ 7.72 (d, J = 8.0 Hz, 4H), 7.27 (d, J = 8.0 Hz, 4H), 4.08–4.06 (m, 4H), 3.60–3.57 (m, 4H), 3.46 (s, 4H), 2.38 (s, 6H). Compound **2**: ^{1}H NMR (400 MHz, $CDCl_3$): δ 3.77 (t, J = 6.8 Hz, 4H), 3.52 (s, 4H), 3.26 (t, J = 6.8 Hz, 4H). Compound **3**: ^{1}H NMR (400 MHz, $CDCl_3$): δ 8.37 (dd, J = 6.7, 3.1 Hz, 4H), 7.48 (dd, J = 6.7, 3.1 Hz, 4H), 4.39–4.34 (m, 4H), 4.04–3.99 (m, 4H), 3.85 (dd, J = 8.6, 4.7 Hz, 8H), 3.81 (dd, J = 5.5, 3.4 Hz, 4H), 3.23 (t, J = 6.9 Hz, 4H).

Synthesis of AnMV.[S6] A solution of 4,4-bipyridine (123.7 mg, 0.8 mmol) in CH_3CN (40 mL) was added in portions to the solution of compound **3** (500 mg, 0.7 mmol) in CH_3CN (100 mL) during 3 days. The reaction mixture was maintained at 70 °C for further 4 days. After cooling, the residue was separated by silica gel column chromatography. The counterions were exchanged firstly to PF_6^- using ammonium hexafluorophosphate (NH_4PF_6), and then were exchanged to Br^- using tetrabutylammonium bromide (TBAB) to yield **AnMV** as a purple solid (73 mg, 17%). ^{1}H NMR (400 MHz, DMSO-d_6): δ 9.07 (d, J = 6.7 HZ, 4H), 8.12 (dd, J = 6.7, 3.2 Hz, 4H), 8.09 (d, J = 6.8 Hz, 4H), 7.29 (dd, J = 6.8, 3.1 Hz, 4H), 4.83 (m, 4H), 4.14 (m, 4H), 4.14 (d, J = 4.5 Hz, 4H), 3.86 (d, J = 3.5 Hz, 8H), 3.80 (m, 4H). ^{13}C NMR (100 MHz, DMSO-d_6): δ 147.41, 146.89, 146.23, 135.88, 125.54, 124.81, 122.92, 75.48, 70.36, 68.93, 60.70. MALDI-TOF: m/z 298.1431 ($[M]^{2+}/2$, calcd for $C_{36}H_{40}N_2O_6^{2+}/2$, 298.1430).

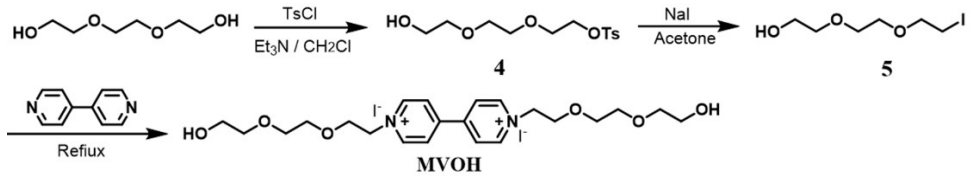

Scheme S2. Synthesis of **MVOH**.

Synthesis of Compound 4, 5, and MVOH. The compounds **4**,[S7] **5**,[S8] and MVOH[S9] were

synthesized according to literature procedures. Compound **4**: ^{1}H NMR (400 MHz, $CDCl_3$): δ 7.78 (d, J = 7.5 Hz, 4H), 7.33 (d, J = 7.7 Hz, 4H), 4.18–4.11 (m, 2H), 3.65–3.71 (m, 4H), 3.59 (s, 4H), 3.56–3.55 (m, 2H), 2.43 (s, 3H). Compound **5**: ^{1}H NMR (400 MHz, $CDCl_3$): ^{1}H NMR (400 MHz, $CDCl_3$): 3.75-3.70 (m, 4H), 3.67-3.63 (m, 4H), 3.59-3.58 (m, 2H), 3.25-3.22 (m, 2H). **MVOH:** ^{1}H NMR (400 MHz, D_2O): δ 9.05 (d, J = 6.0 Hz, 4H), 8.48 (d, J = 9.2 Hz, 4H), 4.82 (d, J = 4.0 Hz, 4H), 4.01 (d, J = 3.8 Hz, 4H), 3.60 (t, J = 4.8 Hz, 4H), 3.58–3.54 (m, 8H), 3.48 (d, J = 3.9 Hz, 4H).

3. Characterization of Complex

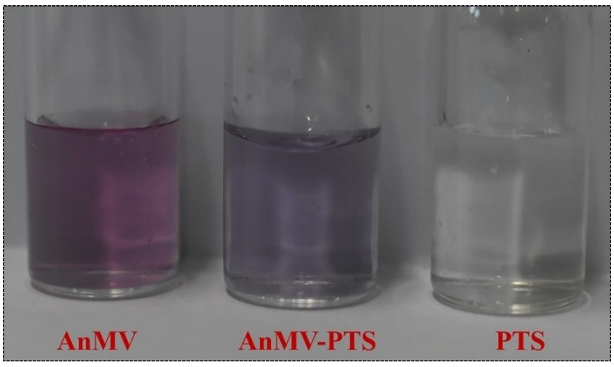

Figure S1. The photographs of **AnMV**, **AnMV–PTS** complex, and **PTS** in aqueous solutions at 0.5 mM.

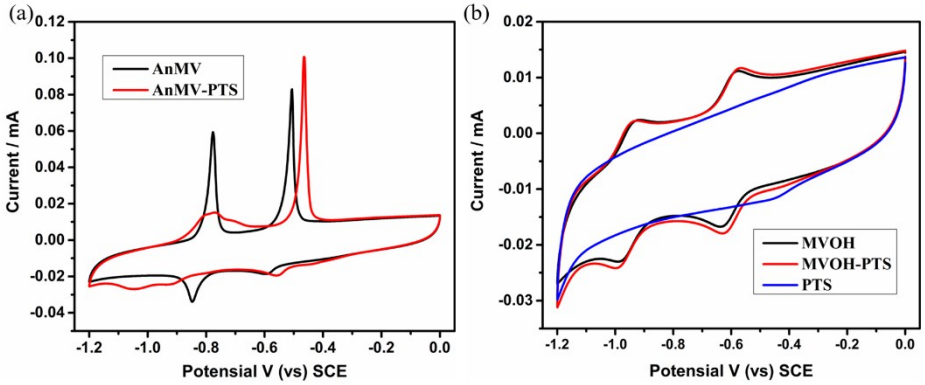

Figure S2. Cyclic voltammograms of (a) free **AnMV** and **AnMV–PTS** complex, and (b) free **MVOH**, **MVOH** with **PTS**, and free **PTS**, in phosphate buffer solution (1 mM, pH 7.0). Scan rate: 100 mV/s. The concentrations of all the constituents were 0.5 mM.

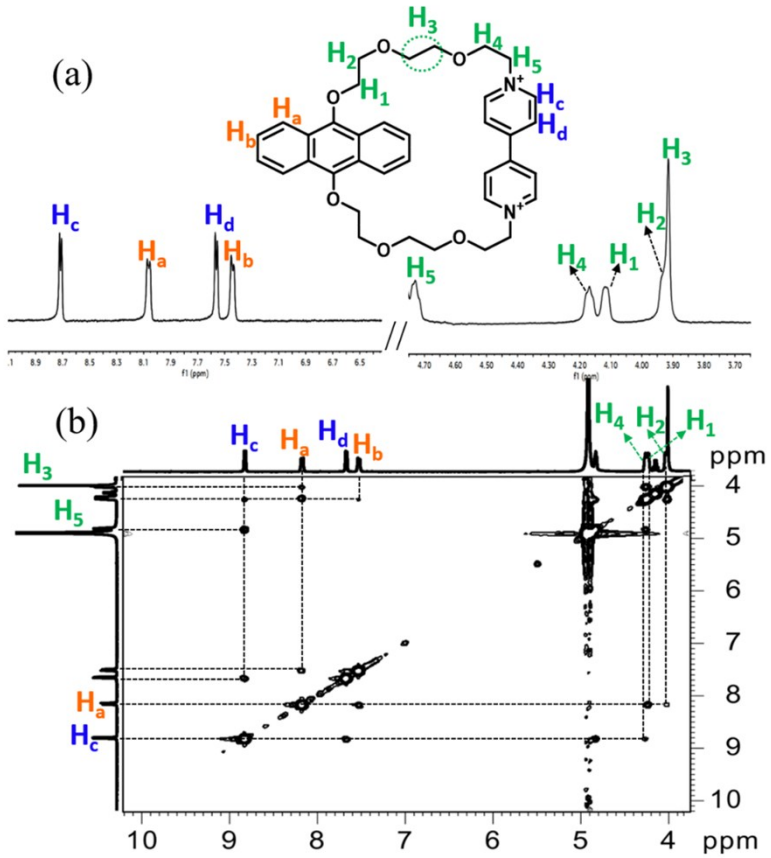

Figure S3. (a) ^{1}H NMR spectrum and (b) ^{1}H–^{1}H NOESY NMR spectrum of **AnMV**. Four peaks appearing in the low field region (7.0 ppm to 9.0 ppm) were assigned to the protons of **An** and **MV** units of **AnMV**. According to the NOE correlations (i.e., H_a with H_1/H_2, and H_c with H_4/H_5), the protons of glycol chain were also clearly assigned. Note that a weak correlation between H_b and H_1 was also observed, possibly because the intramolecular CT interaction forced the **An** unit to twist and to parallelly aligned with the **MV** unit.

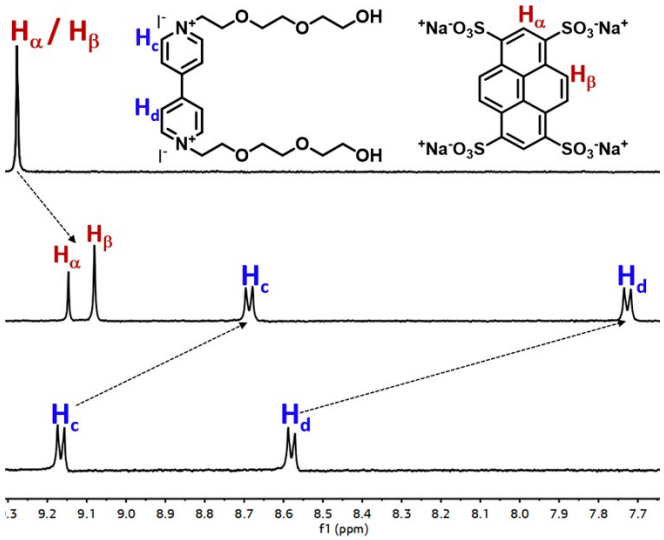

Figure S4. Partial ^{1}H NMR spectra of **MVOH**, **PTS** and **MVOH–PTS** complex (400 MHZ, 0.5

mM).

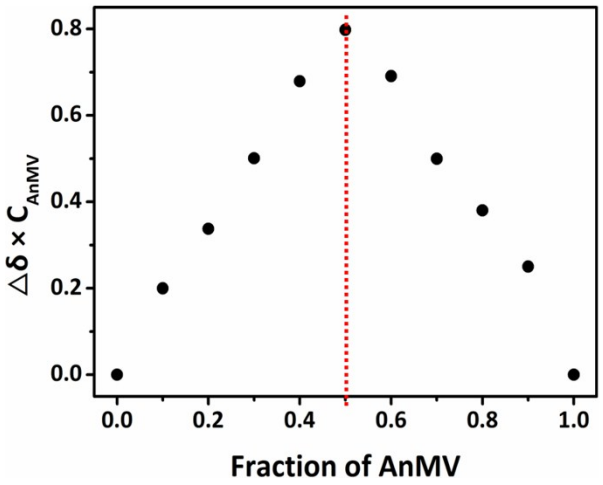

Figure S5. Job plot for the **AnMV–PTS** system. [**AnMV**] + [**PTS**] = 1.0 mM.

	D_0 (Diffusion coefficient (m^2 s^{-1})
AnMV-PTS	2.00×10^{-10}
AnMV	2.88×10^{-10}
PTS	2.95×10^{-10}

Table S1. Diffusion coefficients of **AnMV–PTS** complex, free **AnMV**, and free **PTS**. The hydrodynamic volume ratios of **AnMV–PTS** complex and free **AnMV** can be calculated with Stokes-Einstein equation by the ratio of diffusion coefficients.

$$D = k_b T / 6\pi\eta R, \quad \left(\frac{D_{AnMV}}{D_{AnMV-PTS}}\right)^3 = \left(\frac{R_{AnMV-PTS}}{R_{AnMV}}\right)^3 = \frac{V_{AnMV-PTS}}{V_{AnMV}}$$

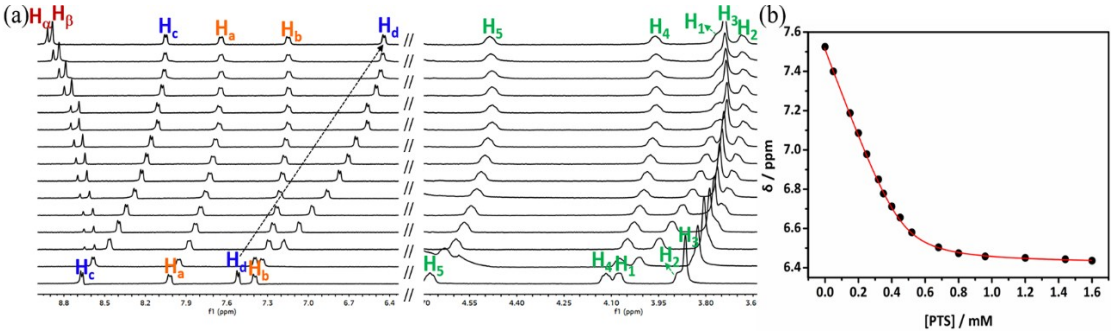

Figure S6. (a) Partial ^{1}H NMR spectra of **AnMV** recorded at a concentration of 0.50 mM with different concentrations of **PTS**: 0.00 mM, 0.05 mM, 0.15mM, 0.20 mM, 0.25 mM, 0.29 mM, 0.32 mM, 0.36 mM, 0.40 mM, 0.44 mM, 0.53 mM, 0.67 mM, 0.80 mM, 0.96 mM, 1.20 mM, and 1.60 mM. (b) Chemical shift changes of H_b on **AnMV** (0.5 mM) observed upon addition of **PTS**. The red line was obtained from non-linear curve-fitting.

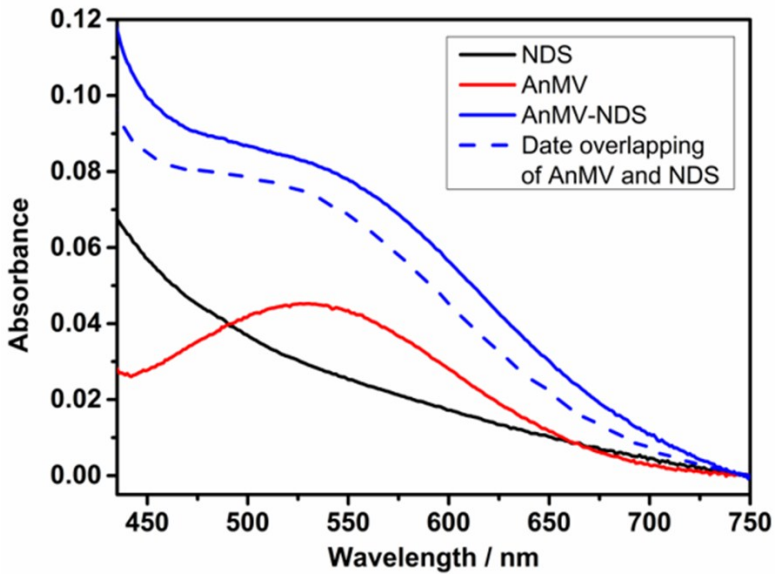

Figure S7. UV−vis absorption spectra of **NDS**, **AnMV** and **AnMV−NDS** in aqueous solution. The concentrations were 0.1 mM for **AnMV**, and 50 mM for **NDS**.

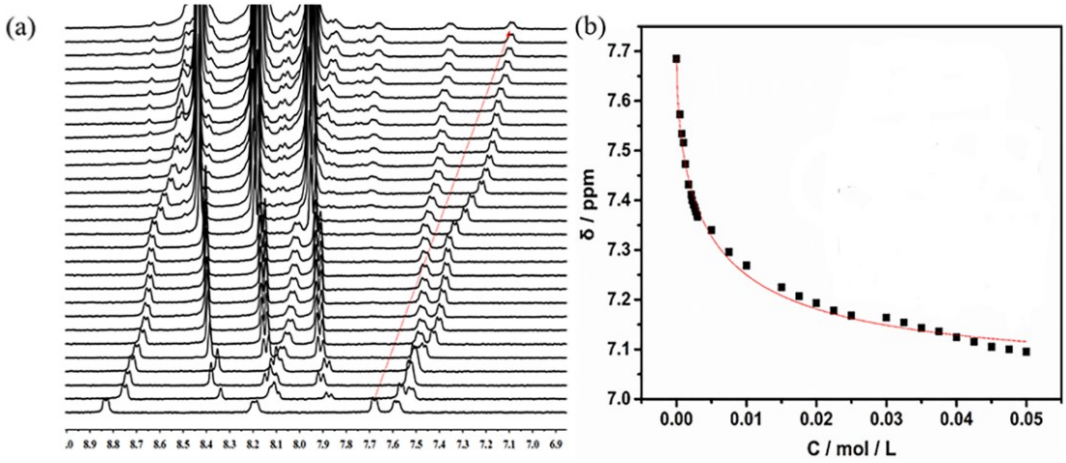

Figure S8. (a) Partial ^{1}H NMR spectra of **AnMV** recorded at a concentration of 0.50 mM with different concentrations of **NDS**: 0.00 mM, 0.50 mM, 1.00 mM, 1.50 mM, 2.00 mM, 2.50 mM, 3.00 mM, 4.00 mM, 4.50 mM, 5.00 mM, 7.50 mM, 10.00 mM, 12.50 mM, 15.00 mM, 17.50 mM, 20.00 mM, 22.50 mM, 25.00 mM, 27.50 mM, 30.00 mM, 32.50 mM, 35.00 mM, 37.50 mM, 40.00 mM, 42.50 mM, 45.00 mM, 47.50 mM, and 50.00 mM. (b) Chemical shift changes of H_d on **AnMV** (0.5 mM) observed upon addition of **NDS**. The red line was obtained from non-linear curve-fitting

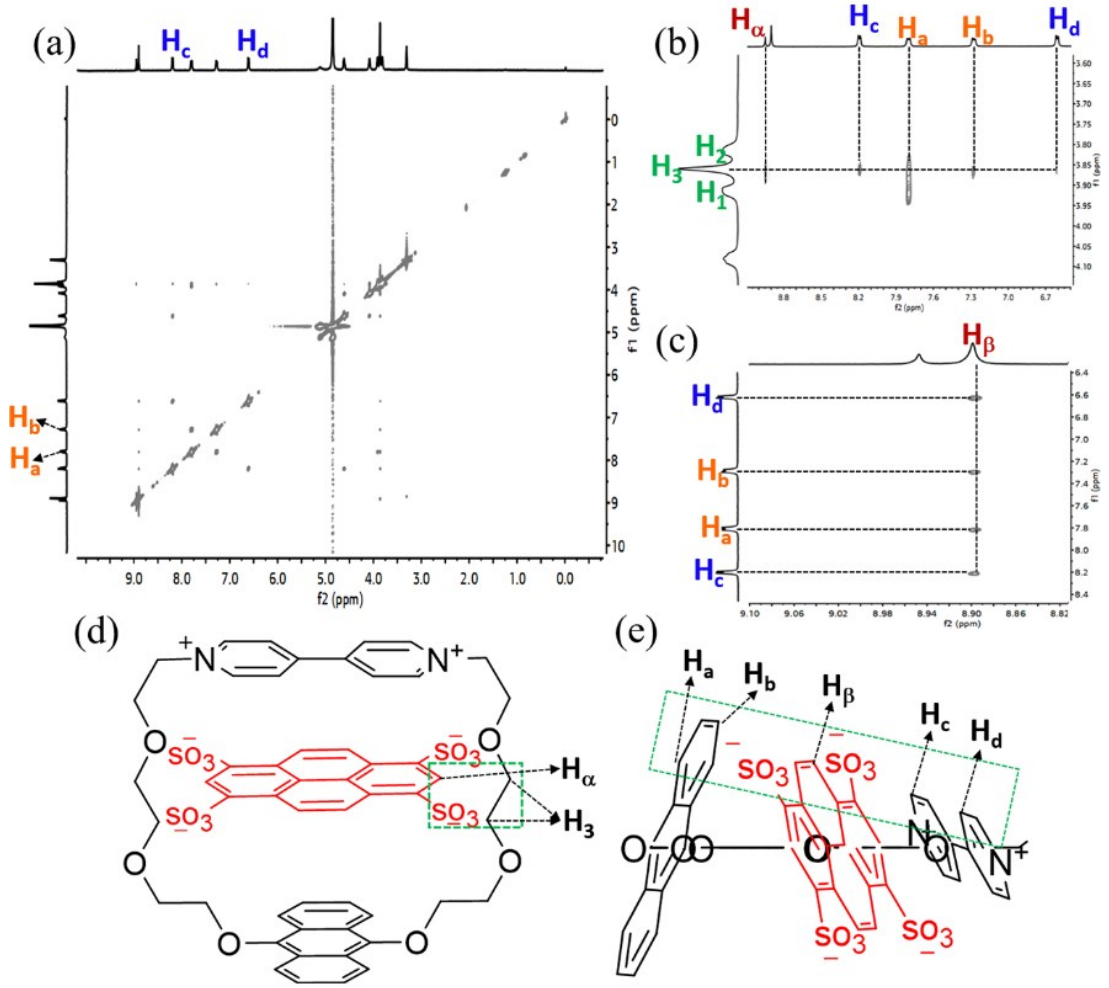

Figure S9. (a) ^{1}H–^{1}H NOESY NMR spectrum of **AnMV–PTS** complex. Concentrations of all the substances were kept at 1 mM. (b,c) Magnified ^{1}H–^{1}H NOESY NMR spectrum. Note that some weak correlations between H_3 of the glycol chain, and **An** and **MV** segments, which may be due to the rearrangement of the flexible spacer during host-guest complexation. (d,e) The schematic illustration of the geometrical configuration for **AnMV**–**PTS** complex.

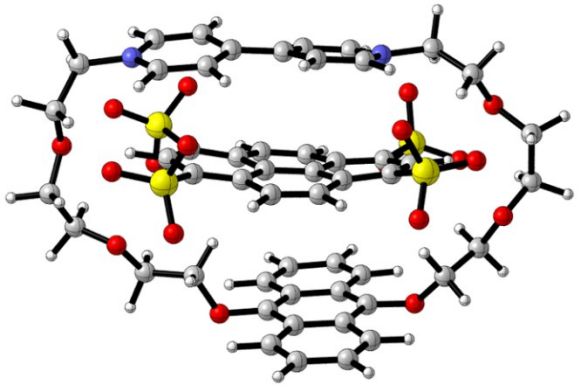

Figure S10. Energy optimized structure of **AnMV**–**PTS** complex.

4. Characterization of Photolysis

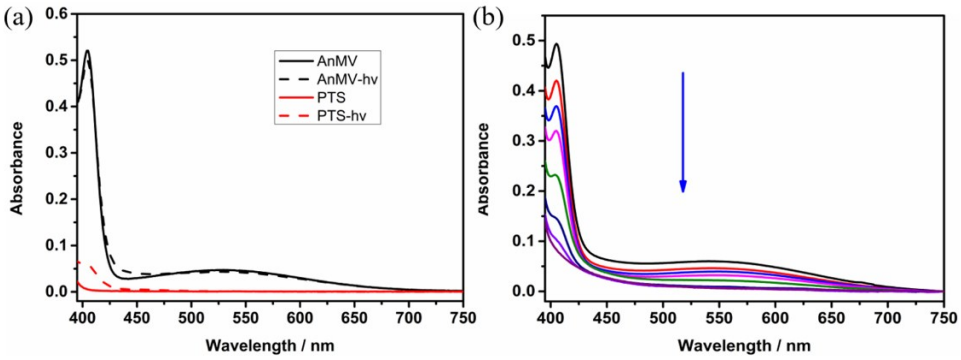

Figure S11. UV−vis absorption spectra of (a) free **PTS** and free **AnMV**, and (b) **AnMV–PTS** complex before and after irradiation for 60 min. Concentrations of all the substances were kept at 0.1 mM.

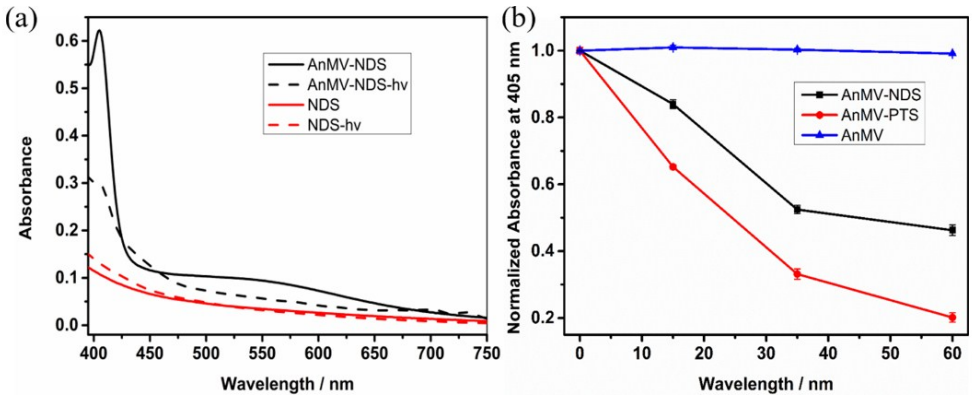

Figure S12. (a) UV−vis absorption spectra of **AnMV–NDS** complex and free **NDS** before and after light irradiation for 60 min. [**AnMV**] = 0.1 mM, [**NDS**] = 50 mM. (b) Normalized absorbance at 405 nm of the **AnMV–NDS** complex, **AnMV–PTS** complex, and free **AnMV** upon light irradiation for different times.

5. Characterization of Photolytic Products

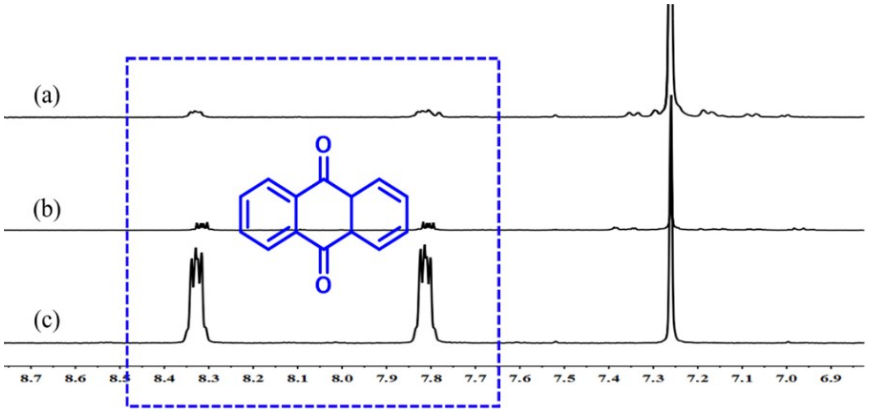

Figure S13. ^{1}H NMR spectra ($CDCl_3$) of the photolytic products of (a) **AnMV–PTS** complex, and (b) **AnMV** in the extracted organic phase. (c) ^{1}H NMR spectrum ($CDCl_3$) of 9,10-anthraquinone.

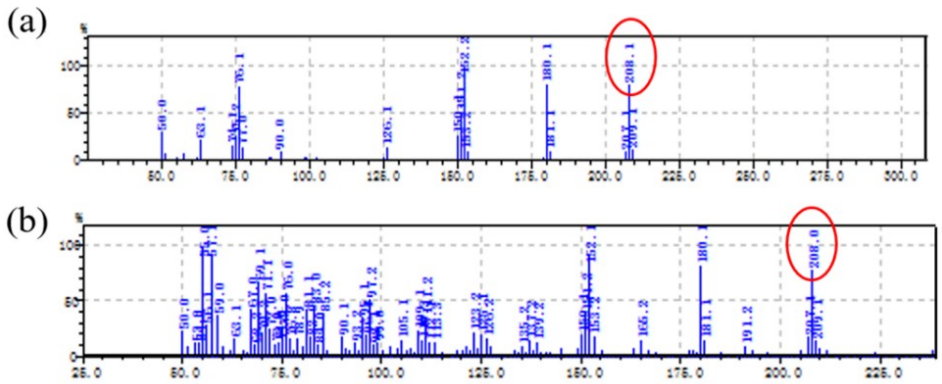

Figure S14. GC-MS spectra of the photolytic products of (a) **AnMV**, and (b) **AnMV–PTS** complex in the extracted organic phase.

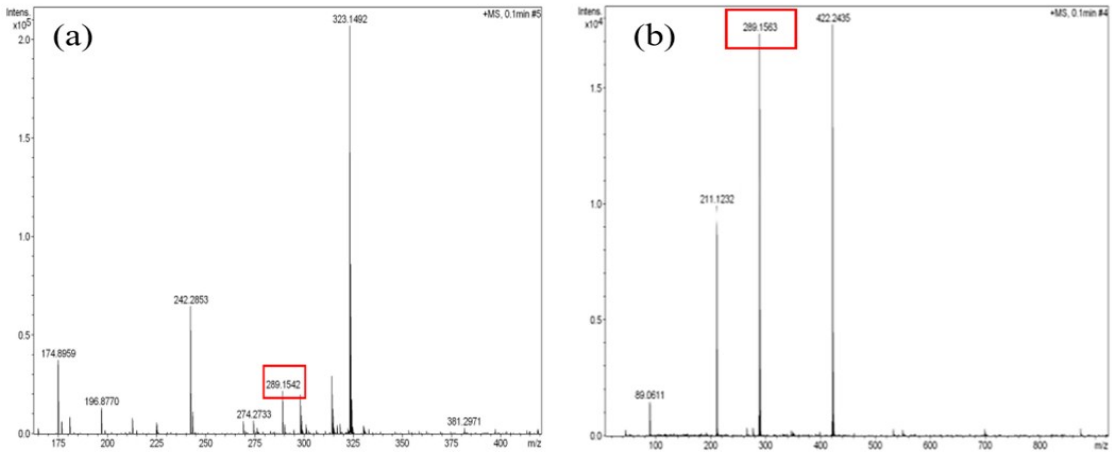

Figure S15. HR-ESI-MS spectra of (a) the photolytic product of **AnMV–PTS** complex in the extracted aqueous phase, and (b) **MVOH**.

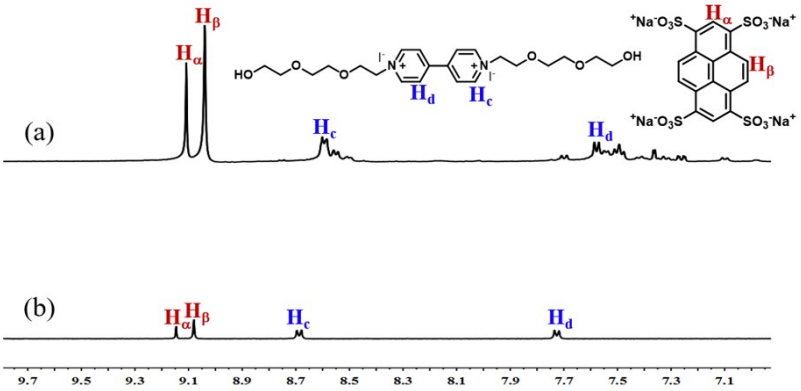

Figure S16. Partial ^{1}H NMR spectra (D_2O) of (a) the photolytic products of **AnMV–PTS** complex in the extracted aqueous phase, and (b) **PTS** with **MVOH**.

6. Characterization of aggregate

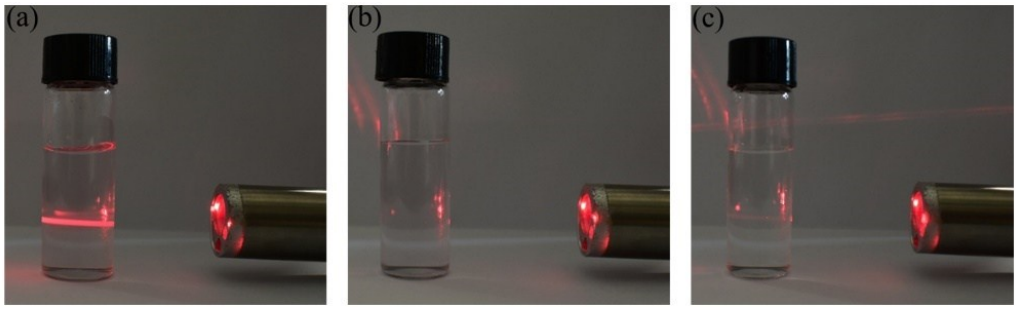

Figure S17. The Tyndall phenomena of (a) **AnMV–PS** complex, (b) **AnMV**, and (c) **PS** in water. Concentrations of all the substances were kept at 0.08 mM.

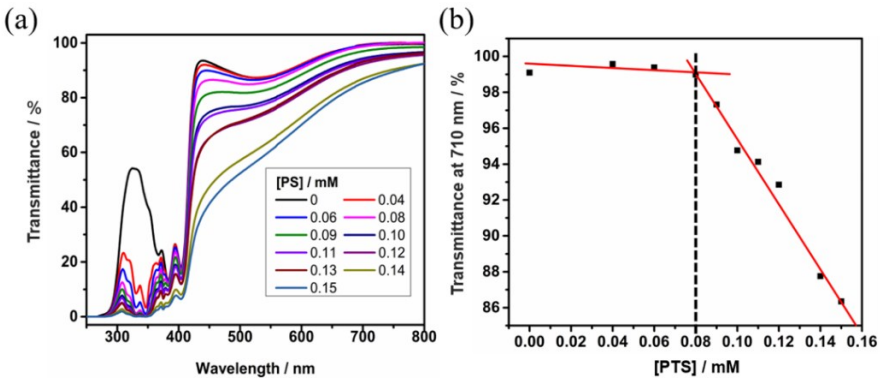

Figure S18. (a) Optical transmittance of **PS** at different concentrations in the presence of **AnMV** (0.15 mM) in water. (b) Dependence of the optical transmittance at 710 nm on the **PS** concentration (0.04-0.15 mM) in the presence of **AnMV** (0.15 mM) in water. It should be noted that: the concentration of **AnMV–PS** complex was kept at 0.1 mM in the subsequent experiments, at which AnMV–PS aggregate showed good colloidal stability.

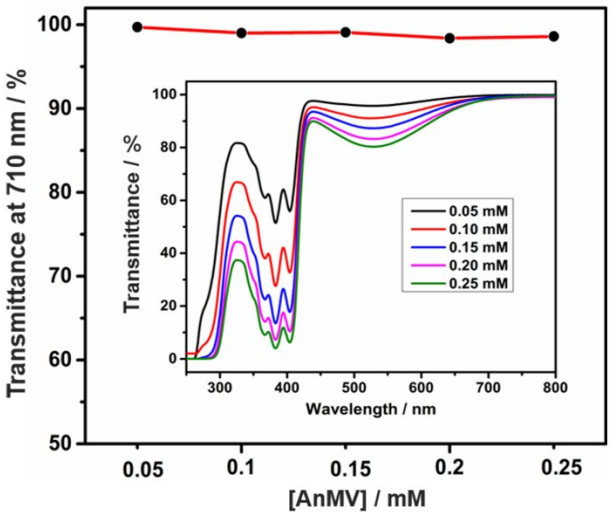

Figure S19. Dependence of the optical transmittance at 710 nm on **AnMV** concentration. Inset: optical transmittance of aqueous solutions of **AnMV** at different concentrations at 25 °C.

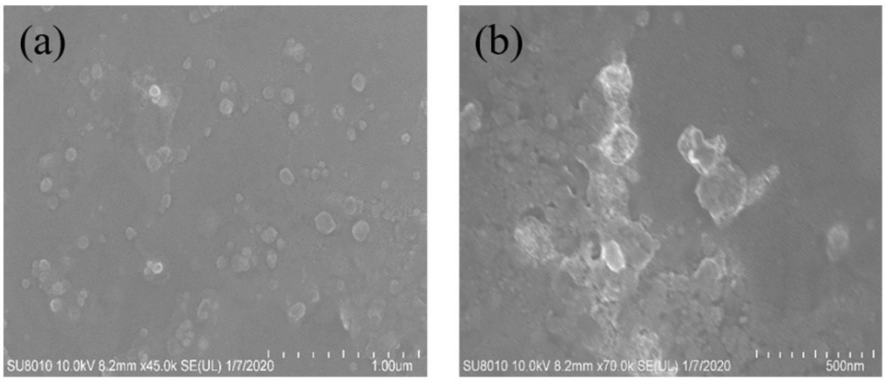

Figure S20. SEM images of **AnMV–PS** aggregate (a) before and (b) after irradiation.

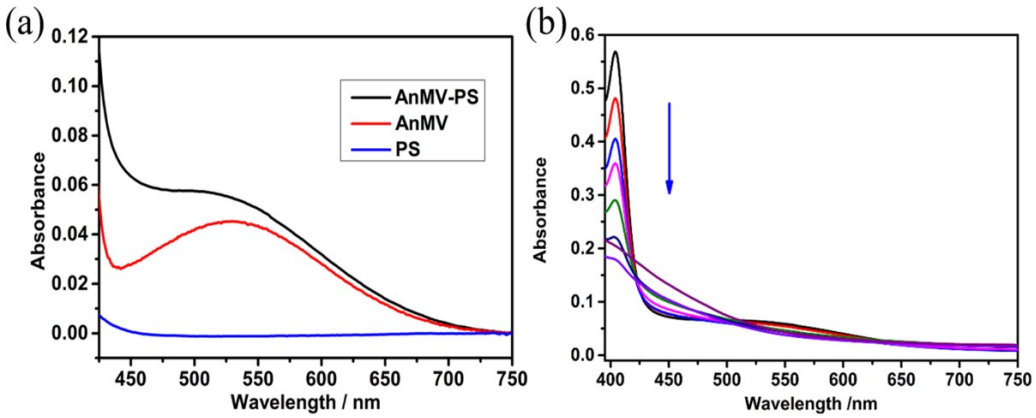

Figure S21. UV–vis absorption spectra of (a) **AnMV–PS**, **AnMV** and **PS** in water, and (b) **AnMV–PS** aggregate before and after irradiation for 60 min. Concentrations of the all substances were kept at 0.1 mM.

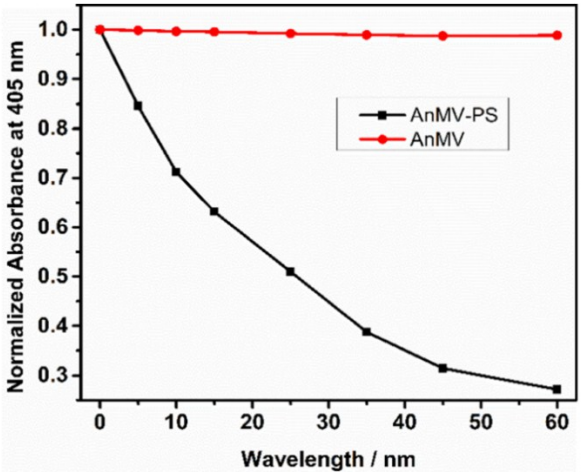

Figure S22. Normalized absorbance at 405 nm of the free **AnMV** and **AnMV−PS** aggregate upon light irradiation for different times. Concentrations of all the substances were kept at 0.1 mM.

7. NMR and Mass spectra

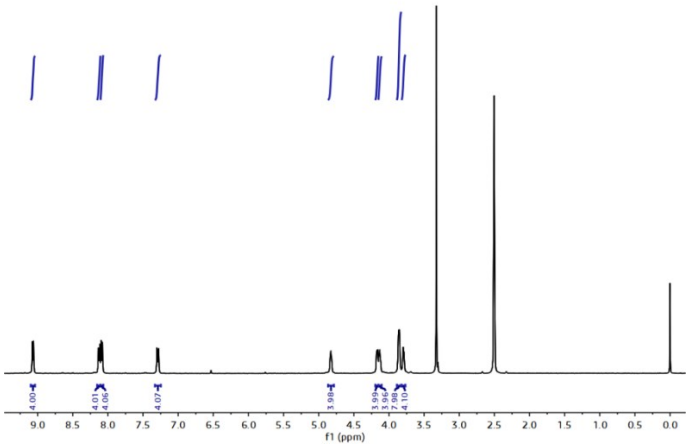

Figure S23. ^{1}H NMR spectrum of compound **AnMV** in DMSO-d_6.

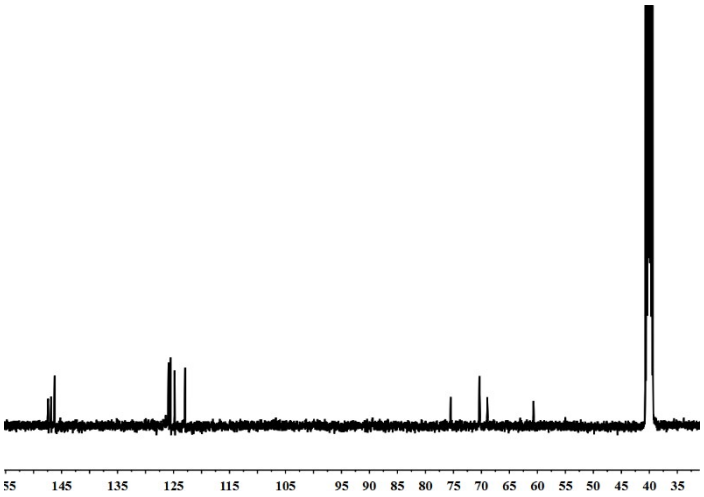

Figure S24. ^{13}C NMR spectrum of compound **AnMV** in DMSO-d_6.

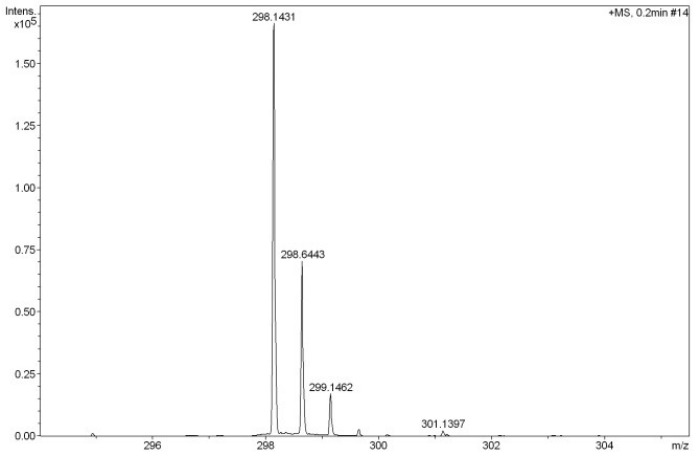

Figure S25. HR-ESI-MS spectrum of compound **AnMV.**

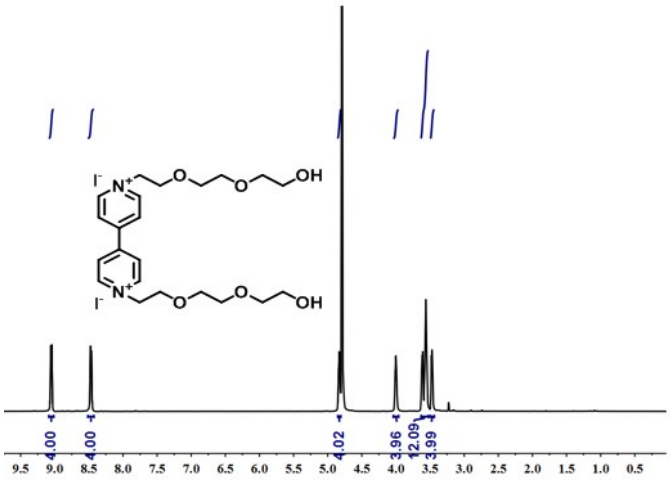

Figure S26. ^{1}H NMR spectrum of compound **MVOH** in D_2O.

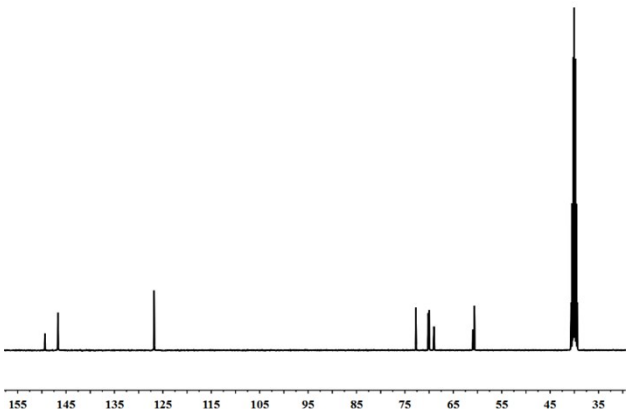

Figure S27. ^{13}C NMR spectrum of compound **MVOH** in DMSO-d_6.

8. Supporting References

S1. M. J. Frisch, G. W. Trucks, H. B. Schlegel, G. E. Scuseria, M. A. Robb, J. R. Cheeseman, G. Scalmani, V. Barone, B. Mennucci, G. A. Petersson, H. Nakatsuji, M. Caricato, X. Li, H. P. Hratchian, A. F. Izmaylov, J. Bloino, G. Zheng, J. L. Sonnenberg, M. Hada, M. Ehara, K. Toyota, R. Fukuda, J. Hasegawa, M. Ishida, T. Nakajima, Y. Honda, O. Kitao, H. Nakai, T. Vreven, J. A., Jr. Montgomery, J. E. Peralta, F. Ogliaro, M. Bearpark, J. J. Heyd, E. Brothers, K. N. Kudin, V. N. Staroverov, R. Kobayashi, J. Normand, K. Raghavachari, A. Rendell, J. C. Burant, S. S. Iyengar, J. Tomasi, M. Cossi, N. Rega, N. J. Millam, M. Klene, J. E. Knox, J. B. Cross, V. Bakken, C. Adamo, J. Jaramillo, R. Gomperts, R. E. Stratmann, O. Yazyev, A. J. Austin, R. Cammi, C. Pomelli, J. W. Ochterski, R. L. Martin, K. Morokuma, V. G. Zakrzewski, G. A. Voth, P. Salvador, J. J. Dannenberg, S. Dapprich, A. D. Daniels, Ö. Farkas, J. B. Foresman, J. V. Ortiz, J. Cioslowski and D. J. Fox, *Gaussian 09*; Gaussian, Inc.: Wallingfor, CT, 2009.

S2. (a) C. T. Lee, W. T. Yang and R. G. Parr, *Phys. Rev. B: Condens. Matter Mater. Phys.,* 1988, **37**, 785–789; (b) A. D. Becke, *J. Chem. Phys.,* 1993, **98**, 5648–5652.

S3. D. L. Mohler and G. Shen, *Org. Biomol. Chem.*, 2006, **4**, 2082–2087.

S4. M. Jensen, S. Schmidt, N.-U. Fedosova, J. Mollenhauer, H.-H. Jensen, *Bioorg. Med. Chem.*, 2011, **19,** 2407–2417.

S5. D. Arian, L. Kovbasyuk and A. Mokhir, *J. Am. Chem. Soc.*, 2011, **133**, 3972–3980.

S6. T.-J. Qian, F.-Y. Chen, Y.-L. Chen, Y.-X. Wang, and W.-P. Hu, *Chem. Commun.*, 2017, **53**, 11822-11825.

S7. P. Iqbal, F. J. Rawson, W. K.-W. Ho, S.-F. Lee, K. C.-F. Leung, X. Wang, A. Beri, J. A. Preece, J. Ma and P. M. Mendes, *ACS Appl. Mater. Interfaces,* 2014, **6**, 6264-6274.

S8. S. Arumugam, V. -V. Popik, *J. Am. Chem. Soc*., 2011, **133**, 15730–15736.

S9. A.Mirzoian and A. E. Kaifer, *Chem. Eur. J.,* 1997**, 3,** 1052-1058.